International Journal Of
Industrial Electronics Control and Optimization
Print ISSN: 3517-2645
Online ISSN: 3568-2645
Homepage: https://ieco.usb.ac.ir/

# Particle Filter Design for Fuel Temperature and Precursor Concentration Estimation under Different Power Conditions in a Nuclear power plant

Hossein Zahmatkesh[1] | Hussein Eliasi[2]

Faculty of Electrical and Computer Engineering, University of Birjand, Birjand, Iran.[1,2]
Corresponding author's email: h_eliasi@birjand.ac.ir

**Article Info**

**Article type:**
Research Article

**Article history:**
Received: 10-November-2024
Received in revised form: 16-January-2025
Accepted:08-February-2025
Published online: 23-Sep-2025

**Keywords**:
Pressurized Water Reactor,
Precursors concentrations,
Kalman filter (KF),
Extended Kalman filter (EKF),
Particle filter (PF).

**ABSTRACT**

State estimation of nuclear reactors often plays a crucial role in accomplishing load-following control. This study presents a novel approach that leverages a weighted particle filter to address the challenges associated with estimating these crucial parameters, including relative precursor concentration ($C_r$) and fuel temperature ($T_f$), under varying reactor power conditions. A high-fidelity nonlinear dynamic reactor model was developed, incorporating noises in both process and measurement models. The proposed method was evaluated by extensive simulations under a wide range of operational scenarios. The particle filter demonstrated exceptional performance in tracking the time-varying states of the nuclear reactor. Comparative analysis with a conventional Kalman filter and the extended Kalman filter revealed the superior robustness of the particle filter in handling nonlinearities inherent in nuclear systems. The proposed approach offers several advantages, including the ability to capture multimodal distributions, handle non-Gaussian noise, and provide probabilistic estimates. Despite the increased computational cost associated with particle filtering, the benefits in terms of estimation accuracy and reliability justify its application in nuclear power plant monitoring and control systems.

## I. Introduction

Nuclear power plants are essential to the global energy landscape, providing a reliable and low-carbon source of electricity. However, these complex systems exhibit nonlinear behaviors, making their operation intricate and demanding precise control. Parameters such as precursor concentration and fuel temperature are crucial for maintaining reactor stability and preventing accidents. Accurate estimation of these parameters is vital for optimizing plant performance, ensuring safety, and extending the lifespan of nuclear fuel. By leveraging advanced modeling techniques and real-time monitoring, engineers can gain valuable insights into the reactor's internal state, enabling proactive decision-making and timely interventions [1].

Precursor concentration and fuel temperature play a pivotal role in reactor dynamics, influencing factors such as reactivity, power distribution, and thermal-hydraulic conditions. However, the radioactive environment within the reactor core renders direct measurement of these quantities exceedingly difficult, if not impossible. Consequently, advanced estimation techniques, such as those based on mathematical models and statistical inference, are essential for inferring these critical states from available sensor measurements. By employing these techniques, we can gain valuable insights into the reactor's internal state, enabling proactive monitoring, control, and decision-making, ultimately enhancing both safety and operational efficiency [2].

Jiuwu Hui [3] researched the application of the Extended State Observer (ESO) for regulating power levels in nuclear power plants. The study aimed to create a control strategy that integrates ESO with Adaptive Dynamic Sliding Mode Control (ADSMC) techniques. This ESO-ADSMC approach effectively tackles the challenges posed by the dynamic behavior and uncertainties inherent in nuclear power plant operations. Qadeer and Bhatti [4] introduced an innovative

technique to estimate the states of automotive engines through a super-twisting second-order sliding mode observer. This observer demonstrated exceptional accuracy in estimating the dynamic states of the system, effectively handling variations and disturbances that may arise during operation.

Jiuwu Hui and Jingqi Yuan [5] suggested the application of a particle filter for accurate linear state estimation in the presence of perturbations within a modular high-temperature gas-cooled reactor. This approach leverages a set of particles to effectively capture and address uncertainties and disturbances, representing the potential states of the system. In 2019, Dong et al. [6] proposed an adaptive state observer designed to estimate the concentrations of poisons in nuclear power plants. This innovative approach utilizes adaptive algorithms to continuously refine estimations by incorporating real-time measurements and the dynamics of the system. In 2018, Ansarifar et al. [7] employed a Higher-Order Sliding Mode Observer (HOSMO) in a Pressurized Water Reactor (PWR) to estimate the nonlinear dynamics of poisons present in a nuclear power plant. The development of the HOSMO, focused on xenon concentration, requires the formulation of a control strategy aimed at maintaining stable and accurate reactor performance in response to varying power demands. Wang et al. [8] explored the application of Artificial Neural Networks (ANNs) to estimate poison concentrations in nuclear power plants. They developed an ANN model by training it with historical operational data, which was then employed for real-time estimation of poison concentrations. Zhe Dong et al. [9] utilized a high-order ESO as a state estimation method to assess state variables and disturbances within energy systems. They particularly focused on nuclear reactors. Koul et al. [10] explored the use of the Rao-Blackwellized unscented Kalman filter for adaptive state estimation in nuclear reactors. This approach merges the advantages of the unscented Kalman filter with the Rao-Blackwellization principle, thereby improving the accuracy and adaptability of state monitoring. In 2015, an Extended Kalman Filter (EFK) was designed by Ansarifar et al. [11]. They used the EKF approach to estimate the poison concentrations and precursor density in a nuclear power plant with three groups of delayed neutrons.

In [12], a study was conducted to estimate dynamic variables in power systems using various Bayesian filters, including the EKF, unscented Kalman filter, ensemble Kalman filter, and particle filter. The study identified that while some filters excelled in accuracy, others offered greater robustness under noisy conditions, highlighting trade-offs in effectiveness and computational complexity. In [13], a novel method was introduced for estimating adhesion in rail systems, combining an EKF with particle swarm optimization. This approach addresses the challenges associated with adhesion estimation and shows that the application of artificial intelligence and machine learning techniques can improve accuracy, offering potential advantages for the rail transport industry. In [14], a novel linear parameter varying estimator was developed to estimate the hydrazine molar concentration in the secondary circuit of nuclear power plants. The proposed method utilizes dynamic shaping filters of arbitrary order to define estimation performance objectives, leveraging $L_2$-gain synthesis based on uncertainty characterization through static integral quadratic constraint multipliers. In [15], a study was conducted to develop a novel approach for reactor power level control in PWRs by integrating Nonlinear Generalized Predictive Control (NGPC) with an EKF. The research demonstrated that this NGPC + EKF methodology could effectively address the challenges of nonlinearity, model mismatch, and noise and significantly enhance the reliability and performance of nuclear reactor control systems. This innovative approach represents a valuable advancement in nuclear engineering.

By incorporating the particle filter approach into our estimation framework, we aim to address the difficulties related to the precise estimation of fuel temperature and precursor concentrations within a nuclear power plant setting. Our research seeks to enhance both the accuracy and reliability of these concentration estimates significantly. The results from our simulations provide strong support for the effectiveness of the proposed observer. Additionally, a comprehensive assessment of the particle filter, along with the Kalman filter and EKF, demonstrates significant improvements in tracking actual system variables and greater resilience to noises. The particle filter, in particular, shows exceptional capabilities in effectively mitigating noises, illustrating its superior performance [16].

The article is organized into a structured framework as follows: Section II introduces a comprehensive mathematical model for the PWR. Section III provides detailed design procedures for the KF, EKF, and PF algorithms with a focus on the estimation of the states within the PWR system. Section IV presents numerical simulations that assess and compare the estimation performance of the different approaches. Finally, Section V concludes with a summary of the key findings.

## II. PWR Formulation

A nuclear reactor model is a sophisticated mathematical representation that encapsulates the physical characteristics and dynamic behavior of a nuclear reactor system. These models are vital for simulating the performance of nuclear reactors under various operational scenarios, providing insights into their efficiency, safety, and overall functionality. The development of these models typically involves a blend of fundamental physical principles, empirical data, and engineering approximations to accurately capture the intricacies of reactor operation [17].

**Assumption 1**: The groups of precursors are considered as a single group. This assumption is made to simplify the model and facilitate the analyses, which will allow for the examination of the overall behavior of these groups rather than the separate effects of the individual precursors.

### *A. Representation of PWR Equations*

In nuclear power plants, the term "neutronics" pertains to the investigation of neutron behavior and interactions within the reactor core. The dynamics of neutrons are governed by a series of equations known as the neutron transport equations. These equations detail the movement of neutrons through the reactor core while considering factors such as neutron production, absorption, scattering, and leakage. A one-point kinetic nuclear reactor model is mathematically represented by the following equations [18], [19]:

$$\frac{dn_r}{dt} = \frac{(\rho - \beta)}{\Lambda} n_r + \frac{\beta}{\Lambda} C_r \tag{1}$$

$$\frac{dC_r}{dt} = \lambda n_r - \lambda C_r \tag{2}$$

where $n_r$ denotes the relative changes in neutron density compared to its initial value, $C_r$ is the delayed neutron precursor concentration, normalized with respect to its initial value, $\beta$ and $\lambda$ denote one group delayed neutron yield and decay constant, respectively, and $\Lambda$ denotes prompt neutron lifetime. Reactor nominal power is outlined below:

$$p(t) = p_0 n_r \tag{3}$$

where $p_0$ denotes the first changes in reactor power level. Xenon poison is the most significant poison in nuclear reactors. For a one-dimensional model of a nuclear reactor core, the fluctuations of this poison can lead to a power plant shutdown. The production rate of this poison has a significant effect on the power of the reactor. The equations of poisons in the nuclear power plant, which include I-135 and X-135, can be expressed as follows [20]:

$$\frac{dI}{dt} = \gamma_I \Sigma f \phi - \lambda_I I \tag{4}$$

$$\frac{dX}{dt} = (\gamma_x \Sigma f - \sigma_x X)\phi - \lambda_x X + \lambda_I I \tag{5}$$

where $I$ and $X$ denote iodine and xenon concentrations respectively, $\sigma_x$ denotes microscopic thermal neutron absorption cross-section of xenon, $\gamma_x$ and $\gamma_I$ denote xenon and iodine yield per fission and $\lambda_x$ and $\lambda_I$ denote xenon and iodine decay constants, respectively, $\Sigma f$ represents the macroscopic fission cross-section, and $\phi$ is the neutron flux represented as follows:

$$\phi = \upsilon n_0 n_r \tag{6}$$

where $\upsilon$ and $n_0$ denote the mean velocity of thermal neutron and initial equilibrium neutron density, respectively. By incorporating the influence of both fuel and coolant temperatures, it is possible to construct a simplified lumped parameter model to analyze thermal transients. The presented model is outlined as follows: [21], [22]:

$$\frac{dT_f}{dt} = \frac{1}{\mu_f}\left[f_f p - \Omega(T_f - T_C)\right] \tag{7}$$

$$\frac{dT_C}{dt} = \frac{1}{\mu_c}\left[(1 - f_f)p + \Omega(T_f - T_C) - 2M(T_C - T_{in})\right] \tag{8}$$

where $T_f$, $T_C$ and $T_{in}$ are fuel temperature, coolant average temperature, and coolant inlet temperature, respectively. The parameter $f_f$ is a fraction of reactor power deposited in the fuel. Also, $\mu_f$ , $\mu_c$, $\Omega$, and $M$ are the total heat capacity of the fuel, the total heat capacity of the coolant, the heat transfer coefficient between fuel and coolant, and the mass flow rate multiplied by the heat capacity of the coolant, respectively. The reactivity model $\rho$ of a PWR is influenced by the control rod movement, xenon, and temperature feedback. This model includes the sum of three components where $\delta\rho_{ext}$ represents reactivity caused by control rod movement, $\delta\rho_T$ denotes thermal reactivity feedback referring to the change in reactivity due to changes in temperature, and $\delta\rho_X$ denotes variations in xenon concentration which lead to alterations in feedback reactivity. The one-point reactivity model is depicted as follows:

$$\rho = \delta\rho_{ext} + \delta\rho_T + \delta\rho_X \tag{9}$$

where

$$\frac{d(\delta\rho_{ext})}{dt} = G_r Z_{rod} \tag{10}$$

$$\delta\rho_T = \alpha_f(T_f - T_{f0}) + \alpha_C(T_C - T_{C0}) \tag{11}$$

$$\delta\rho_X = -\frac{\sigma_X(X - X_0)}{\sum f} \tag{12}$$

where $G_r$ and $Z_{rod}$ denote the total reactivity of the control rod and control rod speed. $\alpha_f$ and $\alpha_C$ denote the thermal reactivity coefficient of the fuel and coolant, respectively. $T_{f0}$, $T_{C0}$ and $X_0$ denote the initial conditions of fuel temperature, liquid coolant temperature, and xenon, respectively. The above equations should be written as (13-18) to adhere to the framework of state equations [12].

$$\dot{x} = f_C(x, u) + w_c$$
$$y = h_C(x, u) + v_c \tag{13}$$

$$E[w_c w_c^T] = Q \tag{14}$$

$$E[v_c v_c^T] = R \tag{15}$$

$$x = [n_r, C_r, I, X, T_f, T_c, \delta\rho_{ext}]^T \tag{16}$$

$$u = Z_{rod} \tag{17}$$

$$y = n_r \tag{18}$$

where x is the state vector, y is the output vector, u is the input vector, the functions $fc$ and $hc$ represent the state and output equations, respectively, and the subscript $c$ indicates

TABLE I NOMENCLATURE

| Parameters | Symbols |
|---|---|
| Initial neutron density | $n_{r0}$ |
| Initial nominal power | $p_0$ |
| Initial equilibrium neutron density | $n_0$ |
| Mean velocity of thermal neutron | $v$ |
| Effective prompt neutron lifetime | $\Lambda$ |
| Fraction of delayed neutron production | $\beta$ |
| Radioactive decay constant | $\lambda$ |
| I-135 decay constants | $\lambda_I$ |
| X-135 decay constants | $\lambda_x$ |
| Total reactivity of the control rod | $G_r$ |
| Fuel total heat capacity | $\mu_f$ |
| Coolant total heat capacity | $\mu_c$ |
| Fraction of reactor power deposited in the fuel | $f_f$ |
| Inlet coolant temperature | $T_{in}$ |
| Macroscopic fission cross-section | $\Sigma_f$ |
| I-135 yield per fission | $\gamma_I$ |
| X-135 yield per fission | $\gamma_x$ |
| Combined effect of mass flow rate and heat capacity of the coolant | $M$ |
| Heat transfer coefficient fuel-to-coolant | $\Omega$ |
| X-135 microscopic absorption cross-section | $\sigma_x$ |
| Thermal reactivity coefficient of fuel | $\alpha_f$ |
| Thermal reactivity coefficient of coolant | $\alpha_C$ |
| Initial condition of liquid coolant temperature | $T_{c0}$ |
| Initial condition of fuel temperature | $T_{f0}$ |
| Initial condition of xenon | $X_0$ |
| Control rod speed | $Z_{rod}$ |
| Average liquid coolant temperature | $T_c$ |
| Fuel temperature | $T_f$ |
| Xenon concentration | $X$ |
| Iodine concentration | $I$ |
| Neutron flux | $\Phi$ |

TABLE II VALUES OF THE PWR PARAMETERS

| Symbols | Values | Units |
|---|---|---|
| $n_{r0}$ | 1 | - |
| $p_0$ | 2500 | $MW$ |
| $n_0$ | $\frac{p_0}{2500} \times (2.5 \times 10^8)$ | - |
| $v$ | $2.2 \times 10^5$ | $cm/s$ |
| $\Lambda$ | $2 \times 10^{-5}$ | $s$ |
| $\beta$ | $6.019 \times 10^3$ | - |
| $\lambda$ | 0.150 | $s^{-1}$ |
| $\lambda_I$ | $2.88 \times 10^{-5}$ | $s^{-1}$ |
| $\lambda_x$ | $2.08 \times 10^{-5}$ | $s^{-1}$ |
| $G_r$ | $14.5 \times 10^{-3}$ | - |
| $\mu_f$ | 26.3 | $MW.s/℃$ |
| $\mu_c$ | $\left(\frac{160}{9} n_{r0} + 540\right)$ | $MW.s/℃$ |
| $f_f$ | 0.92 | - |
| $T_{in}$ | 291.3 | ℃ |
| $\Sigma_f$ | 0.3358 | $cm^{-1}$ |
| $\gamma_I$ | 0.0639 | - |
| $\gamma_x$ | 0.00228 | - |
| $M$ | $(28 \times n_{r0}) + 74$ | $MW.C^{-1}$ |
| $\Omega$ | $\left(\frac{5}{3} n_{r0} + 4.93\right)$ | $MW.C^{-1}$ |
| $\sigma_x$ | $2.36 \times 10^{-18}$ | $cm^2$ |
| $\alpha_f$ | $(n_{r0} - 4.24) \times 10^{-5}$ | $\frac{\delta k}{k}$ /℃ |
| $\alpha_C$ | $(-4n_{r0} - 17.3) \times 10^{-5}$ | $\frac{\delta k}{k}$ /℃ |
| $T_{c0}$ | 303.55 | ℃ |
| $T_{f0}$ | 653.80 | ℃ |
| $X_0$ | $8.11 \times 10^{15}$ | - |

the continuous state. $w_c$ and $v_c$ are the process and output noises, respectively, which are modeled as Gaussian (with zero means), and their covariance matrix is defined according to Eq. (14) and (15), respectively, where $E[.]$ is the statistical math expectation. All the parameters of PWR have been described in Table I. Also, Table II presents the parameter values of the reactor model.

### *B. Discretization of PWR Equations*

To implement the proposed filters, the continuous equations of the nuclear reactor must first be discretized [23]. In order to make the equations discrete, the definition of the derivative for the variable x is used as described in Eq. (19).

$$\dot{x} = \frac{x(k) - x(k-1)}{\Delta t_s} \rightarrow x(k) = x(k-1) + \dot{x}\Delta t_s \quad (19)$$

where $\Delta t_s$ is sampling interval and $k$ and $k-1$ are the same as $k\Delta t_s$ and $(k-1)\Delta t_s$. By substituting the aforementioned relationship into the state matrix equations, we arrive at Eq. (20) as follows:

$$x(k) = x(k-1) + \Delta t_s \times (f_C(x,u) + w_c) \quad (20)$$

By simplifying Eq. (20), we obtain the following relation:

$$\begin{aligned} x_k &= f(x_{k-1}, u_{k-1}) \times \Delta t_s + x_{k-1} + w_{k-1} \\ y_k &= h(x_k, u_k) + v_k \end{aligned} \quad (21)$$

the above equations represent the discretized form of a nuclear power plant, which is used to implement the proposed filters.

## III. Preliminary

This section will explore the Kalman filter, the EKF, and the particle filter, which are used to estimate precursor concentration and fuel temperature.

### *A. Kalman filter*

This method is a computational technique based on mathematical principles, designed to accurately estimate the true states of a system by integrating predictions from a mathematical model with sensor measurements. The method consists of two fundamental steps: prediction and update. In the prediction step, the previous state estimate and the system model are utilized to project the current state forward in time, incorporating information about the system's dynamics to create an expected state prediction. During the update process, the Kalman filter computes the Kalman gain, which determines the appropriate weight to be assigned to

the new measurement data versus the predicted state estimate. The steps of the KF method for the nonlinear PWR dynamics are outlined as [24], [11]:

Prediction step:

In Eq. (22) and (23), the state and covariance matrix of the states are predicted.

$$\hat{x}_k^- = A_k \hat{x}_{k-1} + B_k u_k \quad (22)$$

$$P_k^- = A_k P_{k-1} A_k^T + Q_d \quad (23)$$

$$\hat{x}(0) = \bar{x}_0 \quad P(0) = P_0 \quad (24)$$

where $\hat{x}_k^-$ is the prediction at the current time, $\hat{x}_{k-1}$ denotes the state estimation at time $k-1$, Parameter $Q_d$ depicts the process covariance noise, $P_k^-$ represents the covariance matrix which is predicted from the prediction step, parameters $\bar{x}_0$ denotes the initial mean, and $P_0$ represents the initial covariance estimation error.

Update step:

$$\tilde{y}_k = y_k - H\hat{x}_k^- \quad (25)$$

$$K_k = P_k^- H^T (H P_k^- H^T + R_k) \quad (26)$$

$$\hat{x}_k = \hat{x}_k^- + K_k \tilde{y}_k \quad (27)$$

$$P_k = (I - K_k H) P_k^- \quad (28)$$

where $H$ is the measurement matrix. $\tilde{y}_k$ signifies the deviation of the observed measurement $y_k$, and the predicted measurement $H\hat{x}_k^-$. The measurement noise covariance is $R_k$. Kalman gain, denoted by $K_k$, determines the weight or importance given to the measurements relative to the predicted state estimate, $\hat{x}_k$ represents the state estimation, which is adjusted using the Kalman gain and residual measurement, and $P_k$ is the updated covariance matrix of errors. The given nonlinear model is approximated linearly around the operating conditions (equilibrium point): $x_{eq_k}$ and $u_{eq_k}$. $A_k$ denotes the transfer function of states, $B_k$ is the input matrix applied to the input vector $u_k$. $A_k$ and $B_k$ are outlined below:

$$A_k = \left.\frac{\partial f}{\partial x}\right|_{x_{eq_k}, u_{eq_k}} \quad B_k = \left.\frac{\partial f}{\partial u}\right|_{x_{eq_k}, u_{eq_k}} \quad (29)$$

where $f(.)$ is a function of the states and input of the system mentioned in Eq. (21).

### B. Extended Kalman filter (EKF)

The previously described Kalman filter relied on linearization at the equilibrium point, which renders the $A_k$ and $B_k$ matrices invalid. To address this issue, an EKF is employed. The EKF is a widely used technique for state estimation, operating iteratively to estimate system dynamics from a series of noisy measurements. It consists of two main stages: prediction and update. In the prediction phase, the state estimate and its covariance are advanced in time by applying the nonlinear system dynamics. Then, during the update phase, the projected state estimate is adjusted using the new measurement data. This adjustment utilizes the Kalman gain, which is calculated through the linearization of the system and measurement equations [25]. As outlined by the modified Euler's discretization presented in Eq. (21), the EKF estimation process consists of two key steps: prediction and update. The equations governing the EKF are defined as follows [25]:

Prediction step:

$$\hat{x}_k^- = f(\hat{x}_{k-1}, u_{k-1}) + w_{k-1} \quad (30)$$

$$P_k^- = F_{k-1} P_{k-1} F_{k-1}^T + Q_d \quad (31)$$

Update step:

$$\tilde{y}_k = y_k - h(\hat{x}_k^-, u_k) \quad (32)$$

$$K_k = P_k^- H^T (H P_k^- H^T + R_k) \quad (33)$$

$$\hat{x}_k = \hat{x}_k^- + K_k \tilde{y}_k \quad (34)$$

$$P_k = (I - K_k H) P_k^- \quad (35)$$

where $\tilde{y}_k$ represents the measurement residual, $y_k$ and $h(\hat{x}_k, u_k)$ indicate measurement and estimated measurement, respectively, $K_k$ represents the estimator gain, $\hat{x}_k$ and $P_k$ represent updated states and covariance estimates, respectively, $F_k$ represents the variables transition jacobian, and $H_k$ denotes the observation jacobian expressed as follows:

$$F_k = \left.\frac{\partial f(x_k, u_k)}{\partial x}\right|_{\hat{x}_k^-, u_{k-1}} \quad (36)$$

$$H_k = \left.\frac{\partial h(x_k)}{\partial x}\right|_{\hat{x}_k^-, u_k} \quad (37)$$

### C. Particle filter

According to the approaches reviewed in the previous sections, in the Kalman filter, matrices $A_k$ and $B_k$ are constants. So, if the equilibrium point changes, matrices $A_k$ and $B_k$ cannot be used anymore. On the other hand, in the EKF, if the accurate mathematical model of the system is not available, it may be difficult to estimate the states. Therefore, in order to improve the state estimation according to the mentioned limitations, a PF is evaluated for precursor concentration and fuel temperature estimations.

the particle filter is a state estimation technique used for nonlinear systems with high-dimensional state spaces. It estimates the state's posterior probability distribution by using a set of particles. Each particle represents a potential system state, and its weight indicates the likelihood of that state being true. The particle filter overcomes the limitations of the KF and EKF by employing resampling with replacement, addressing particle degeneracy, improving computational efficiency, and providing a better representation of the posterior distribution, particularly in high dimensional spaces. The particle filter utilizes a set of discrete samples with associated weights to approximate a probability distribution function. This representation is described as follows [26], [27]:

$$P(x_k|y_k) \approx \sum_{i=1}^{N} [W_k^i \tilde{\delta}(x_k - x_k^i)] \quad (38)$$

Eq. (38) represents the posterior distribution $P(x_k|y_k)$ of the state $x_k$ given the observations $y_k$ in the context of a particle filter. The equation approximates this posterior distribution as a sum of contributions from $N$ particles, represented by the index $i$. Each particle $x_k^i$ is assigned a weight $W_k^i$, reflecting how likely that particle is given the observations. These weights are updated at each time step to ensure that the particles representing more probable states are emphasized in the approximation and correspond to:

$$\sum_{i=1}^{N} W_k^i = 1 \quad (39)$$

The delta function $\tilde{\delta}(x_k - x_k^i)$ signifies that each particle contributes to the posterior only when the current state $x_k$ matches the value of the particle $x_k^i$. This allows for the representation of the posterior as a weighted sum of discrete points in the state space. This formulation effectively captures the complexities of the posterior distribution in nonlinear and non-Gaussian systems using a finite number of particles. Each particle serves as a sample of the possible states, allowing for flexible and robust estimation of the state variable $x_k$ based on the observations $y_k$. The PF algorithm is succinctly outlined as follows:

Initialization: Start with a collection of samples $\{x^i(0)\}_i^N$ that are stochastically selected from initial state distribution $P(0)$ and let $W_k^i = 1/N,\ i = 1, \dots, N$.

Prediction: For each particle, propagate it forward in time using the system dynamics. This involves applying the state transition function to each particle, considering the process noise. The prediction stage is outlined as:

$$x_k^i = f(x_{k-1}^i, u_{k-1}) + w_{k-1}^i \quad (40)$$

In (40), $w_{k-1}^i$ indicates white noise with covariance $Q$.

Update: Calculate the weight of each particle based on how well it matches the new measurement, which is done using the measurement model and the current measurement. The update step consists of two parts: particle weight and normalization, which are expressed as follows:

Particle weight:

$$W_k^i = P(y_k|x_k^i) W_{k-1}^i \quad (41)$$

Normalization:

$$W_k^i = \frac{W_k^i}{\sum_{i=1}^{N} W_k^i} \quad (42)$$

Resampling:

$$\frac{1}{\sum_{i=1}^{N} W_k^i} < N_{eff_{th}} \quad (43)$$

Resample the particles with replacement, based on their weights. This step aids in discarding particles with diminished weights, thus prioritizing states with higher likelihoods, $N_{eff_{th}}$ is a predetermined threshold and let $W_k^i = 1/N,\ i = 1, \dots, N$.

State estimation:

$$\hat{x}_k = \sum_{i=1}^{N} [x_k^i W_k^i] \quad (44)$$

Set $k = k + 1$ and repeat the process from step (b).

**Assumption 2**: It is assumed that the measurement and process noise are Gaussian distributed, which is a common assumption in filtering techniques.

## IV. Simulation Results

This section compares the designed Kalman Filter (KF) and EKF [11] in the presence of process and measurement noises for a PWR to demonstrate the superiority of the designed Particle Filter (PF). A feedback linearization controller was implemented to regulate the system dynamics, and numerical simulations were carried out using MATLAB/Simulink. Three scenarios for power level changes were considered to evaluate the estimation approaches. To evaluate the performance of the KF, EKF, and PF, three error detection criteria were employed: Integral Absolute Error (IAE), Mean Error (ME), and Root Mean Square Error (RMSE). This section summarizes the assessment of these filters for state estimation. Metrics such as ME, IAE, and RMSE were used to gauge transient estimation and steady-state accuracy. So, 200 particles were used for simulation in the PF. All system initial conditions are deviated by 5% from their nominal values.

$$IAE = \int_0^{\Phi} |e(.)| dt \quad (45)$$

$$ME = \frac{1}{s} \sum_{i=1}^{s} e_i \quad (46)$$

$$RMSE = \sqrt{\frac{1}{s} \sum_{i=1}^{s} (y^i - \hat{y}^i)^2} \quad (47)$$

The symbol $\phi$ represents total simulation time, while $e(.)$ represents the error of estimation associated with it. Parameter $s$ represents sample size, and $y^i$ and $\hat{y}^i$ indicate the true and predicted values, respectively.

### A. The First Scenario

In the first scenario, the reactor is initially operating at its nominal power level, representing an equilibrium state. At the 18-second mark, the power level is decreased to 80% of the nominal value. Subsequently, at the 108-second mark, the power level is increased back to the nominal value. Fig. 1 shows the first power level changes in the nuclear power plant. Figs. 2 and 3 compare the estimated and actual values of the precursor concentration and fuel temperature for the three filters described in Section III.

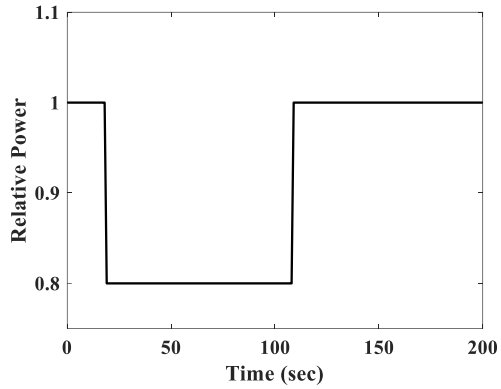


Fig. 1. Relative power changes in the first scenario

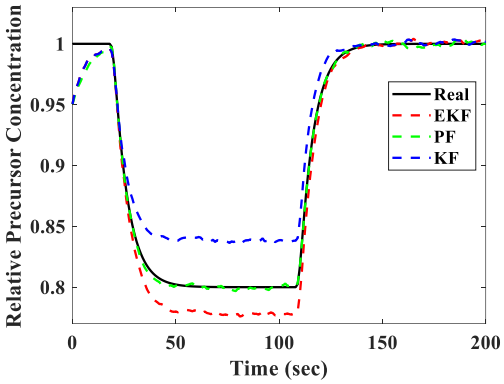


Fig. 2. Precursor concentration estimation with three studied filters

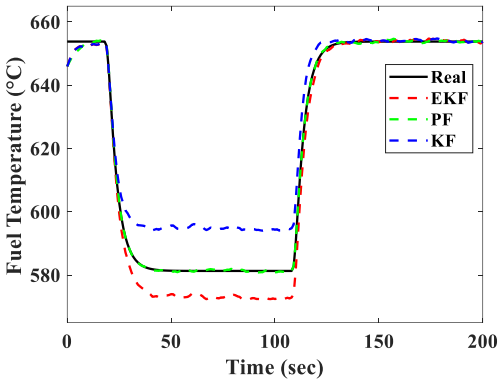


Fig. 3. Fuel temperature estimation with three studied filters

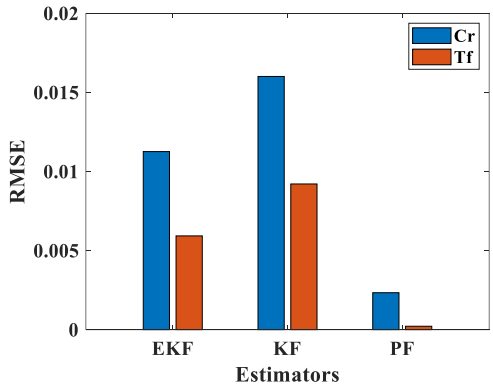


Fig. 4. Comparing RMSE of studied filters in the first scenario

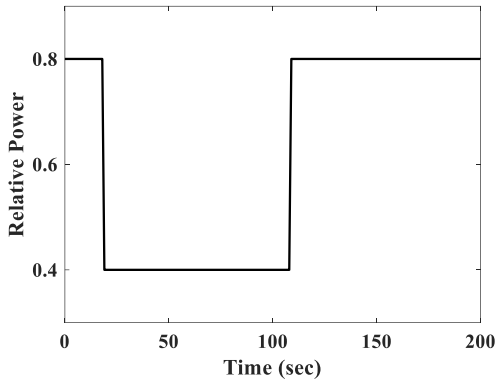


Fig. 5. Relative power changes in the second scenario

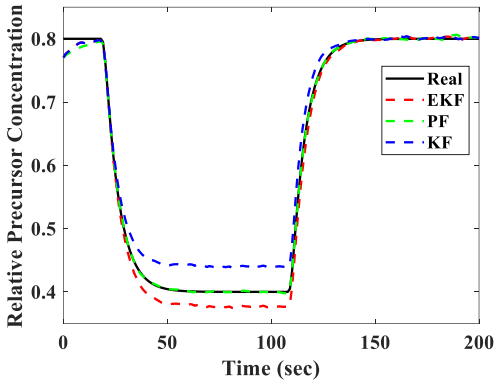


Fig. 6. Precursor concentration estimation with three studied filters

Fig. 4 compares the RMSE of the proposed filters in the first scenario. The results demonstrate that the proposed PF exhibits superior convergence between the estimated and actual states compared to other methods in the first scenario. Furthermore, comprehensive evaluations consistently indicate the superior performance of the PF over both KF and EKF methods.

### *B. The Second Scenario*

In the second scenario, it is assumed that the power of the reactor is at 80% of the rated power. Then, after 18 seconds, the power of the reactor is reduced to 40% of its rated power.

After 108 seconds, the power is increased by 40%. Fig. 5 shows the second power level changes in the nuclear power plant. Figs. 6 and 7 compare the estimated and actual values of the precursor concentration and fuel temperature for the three filters described in Section III. Fig. 8 presents a comparative analysis of the RMSE for the proposed filters under the second scenario. This visualization allows us to directly assess the accuracy of each filter in estimating the true system state, providing valuable insights into their relative performance. The evaluation results indicate that the proposed PF exhibits faster convergence and lower estimation error than the KF and EKF algorithms in the second scenario.

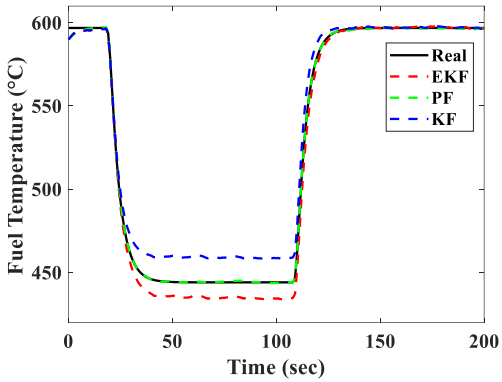


Fig. 7. Fuel temperature estimation with three studied filters

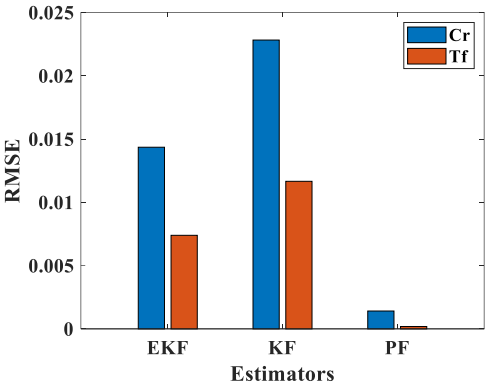


Fig. 8. Comparing RMSE of studied filters in the second scenario

### C. The Third Scenario

In the third scenario, the reactor is subjected to a specific power cycle. It begins operating at 40% of its maximum power capacity. After 18 seconds, the reactor's power output is decreased to 20%. The reactor maintains this reduced power level for 108 seconds before returning to its initial 40% power level. Fig. 9 presents the modeled relative neutron density during this sequence. Fig .10 compares the estimated and the actual value of the precursor concentration for the three filters described in Section III. In addition, Fig. 11 compares the estimated and actual value of the fuel temperature for the three filters. Fig. 12 is a comparative analysis of the RMSE for the proposed filters under the third scenario.

The evaluation results suggest that the proposed PF demonstrates better performance in terms of convergence speed and estimation accuracy when compared to both the KF and EKF algorithms. Specifically, the PF achieves faster convergence, meaning that it reaches accurate estimates more quickly than its counterparts. This characteristic is crucial in applications requiring real-time processing and rapid decision-making. Additionally, the PF exhibits lower estimation errors, which implies that the estimates produced are closer to the true values of the variables being estimated, enhancing overall system reliability.

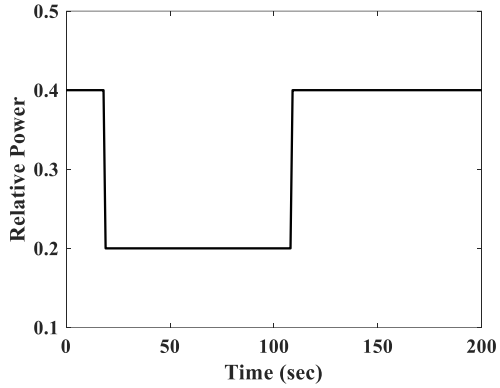


Fig. 9. Relative power changes in the third scenario

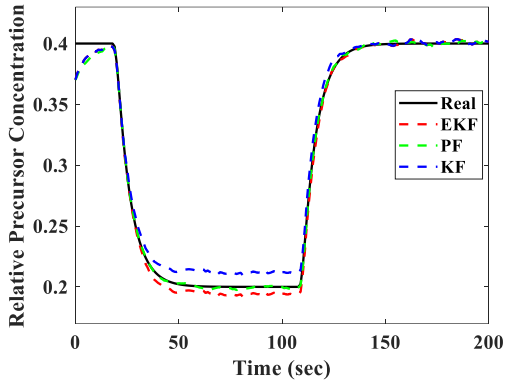


Fig. 10. Precursor concentration estimation with three studied filters

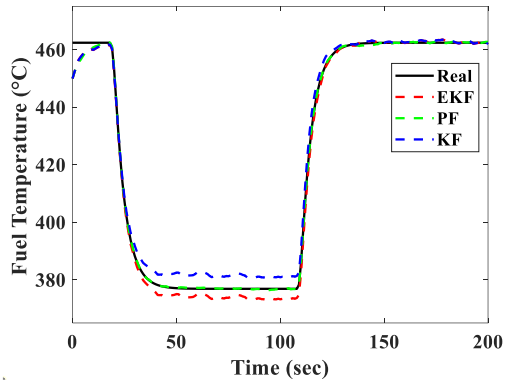


Fig. 11. Fuel temperature estimation with three studied filter

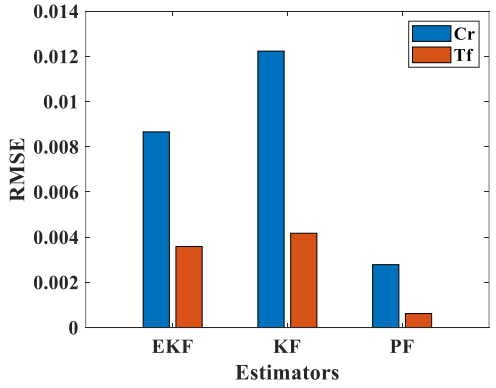


Fig. 12. Comparing RMSE of studied filters in the third scenario

TABLE III OVERVIEW ERROR METRICS FOR PRECURSOR CONCENTRATION AND FUEL TEMPERATURE ESTIMATION AT THREE SCENARIOS

| Powers | Estimation errors | Indices | KF | EKF | PF |
|---|---|---|---|---|---|
| First scenario | $e(C_r)$ | ME | 0.0194 | 0.0119 | 0.0032 |
| | | IAE | 3.8934 | 2.3928 | 0.6380 |
| | $e(T_f)$ | ME | 0.0099 | 0.0062 | 0.00065 |
| | | IAE | 1.9833 | 1.2493 | 0.1317 |
| Second scenario | $e(C_r)$ | ME | 0.0253 | 0.0152 | 0.0032 |
| | | IAE | 5.0925 | 3.0459 | 0.6134 |
| | $e(T_f)$ | ME | 0.0123 | 0.0077 | 0.0007 |
| | | IAE | 3.4774 | 1.5496 | 0.1424 |
| Third scenario | $e(C_r)$ | ME | 0.0173 | 0.0104 | 0.0049 |
| | | IAE | 3.4840 | 2.0834 | 0.9803 |
| | $e(T_f)$ | ME | 0.0058 | 0.0040 | 0.0011 |
| | | IAE | 1.1568 | 0.8131 | 0.2235 |

This study employs two error metrics, ME and IAE, to evaluate the estimation accuracy of precursor concentration and fuel temperature across three power levels. Table III presents the results of the two error metrics, ME and IAE, evaluated across three different scenarios. ME serves as a fundamental metric for assessing the average deviation in estimations, offering insights into the overall accuracy of predictions relative to actual measurements. It is calculated as the average of the differences between predicted values and observed values, helping to identify systematic biases in the estimation model and providing a more comprehensive understanding of the model's performance.

In contrast, IAE offers a more comprehensive analysis of estimation accuracy over time. Unlike ME, which may be misleading in the presence of compensating errors, IAE accumulates the absolute discrepancies, capturing the magnitude of all errors made during the estimation process. By analyzing both ME and IAE, a nuanced understanding of the estimation errors associated with precursor concentration and fuel temperature can be derived, thereby enhancing the reliability of predictive models at varying power levels. One notable drawback of the proposed method is its extended processing time, attributed to its inherent complexity, while alternative methods benefit from shorter processing durations due to their simpler designs. Nevertheless, this trade-off is justified by the superior performance and accuracy of the proposed method, which are critical for ensuring reliable outcomes in our application. Table IV outlines the comparative advantages and disadvantages of the proposed method relative to others.

TABLE IV COMPARISON OF THE PROPOSED METHOD COMPAIR WITH OTHER METHODS

| Method | Advantage | Disadvantage | Processing Time |
|---|---|---|---|
| Particle filter | High Accuracy | Longer processing time | 4.4 sec |
| | Robust performance | | |
| KF and EKF | Faster processing time | Low accuracy | 0.8 sec and 1.37 sec |
| | Simplicity | Limited robustness | |

### *D. Limitations*

One of the limitations identified in this study is the unavailability of comprehensive data on nuclear power plants globally, which hampers the ability to conduct a thorough analysis. This scarcity of data is attributed to several factors, including the diversity of regulatory frameworks in different countries, the proprietary nature of information related to nuclear energy, and the varying levels of transparency associated with national energy policies.

Many nations have imposed strict controls and regulations on the dissemination of information pertaining to nuclear facilities, resulting in fragmented data that can hinder accurate comparisons and assessments. Furthermore, the sensitive nature of nuclear operations often results in limited public access to detailed operational metrics and safety records, which are crucial for comprehensive analysis. Many existing databases either provide outdated information or lack the granularity necessary for robust evaluations of nuclear power plants and their performance. Such challenges underscore the complexities involved in researching nuclear energy infrastructure on a global scale. Therefore, at this stage of the research, reliable data in this area remain unobtainable, which poses significant constraints on the depth and breadth of the analysis that can be undertaken.

Another limitation of this study is the computational cost of the PF. The PF utilizes a set of particles to estimate the state; as the number of particles increases, the accuracy of the estimation improves. However, the computational expense of the PF also rises significantly. The mathematical relationship between the number of particles and the computational load can be expressed as follows:

$$C(N) = k \times N \tag{48}$$

where $C(N)$ represents the computational complexity for $N$ particles and $k$ is a constant value that represents

the amount of computation for each particle. The Eq. (48) illustrates a fundamental characteristic of PFs, where the total computational cost is directly proportional to the number of particles utilized in the estimation process. This linear relationship signifies that as the number of particles increases, the computational demands escalate correspondingly, thereby requiring additional computational resources and time. This understanding emphasizes the trade-off between accuracy and efficiency in particle filtering; while increasing the number of particles can enhance the accuracy of state estimates, it also incurs a substantial increase in computational load. Consequently, careful consideration must be given to the selection of the number of particles in practical applications to achieve a balance between desired accuracy and available computational resources.

## V. Conclusions

This study provided a detailed evaluation of the PF's performance in estimating precursor concentration and fuel temperature, positioning it against both the standard KF and the EKF. The comparison revealed significant advantages of the PF, particularly in terms of accuracy and reliability under different operational scenarios. Three scenarios were analyzed: high power, medium power, and low power. In all three cases, the PF demonstrated a superior ability to minimize estimation errors as defined by RMSE (Root Mean Error), ME (Mean Error), and IAE. These metrics reflect the filter's capacity to closely track the true values of precursor concentration and fuel temperature, particularly during periods of dynamic changes in power levels. The findings highlight the robustness of the PF, especially in high power scenarios where rapid fluctuations are expected. In these conditions, the PF outperformed its Kalman counterparts by efficiently handling the non-linearities and noises associated with the estimation process. In the second and third scenarios, the PF continued to maintain its edge, exhibiting lower error rates and demonstrating better consistency in performance. Furthermore, the ability of the PF to adapt to varying conditions suggests its potential application in more complex systems where precision in estimation is critical.

The results advocate for the adoption of the particle filtering approach in relevant fields, particularly in systems that are subject to rapid changes and unpredictable dynamics. Overall, this study reinforces the importance of advanced filtering techniques in achieving accurate estimations in practical applications. Further investigations could explore the integration of the PF with other methodologies or its application in additional contexts, ensuring continuous improvement in data estimation efforts. This research not only contributes valuable insights into filtering techniques but also emphasizes the ongoing need for innovative solutions in the realm of estimation and control systems.

## Future works

The promising results obtained from the PF in estimating precursor concentration and fuel temperature open several avenues for future research and application. One potential direction is the exploration of hybrid filtering techniques that integrate the strengths of the PF with those of other estimation methods, such as deep learning algorithms or multi-model approaches. By leveraging the adaptive capabilities of these methodologies, it may be possible to further enhance estimation accuracy in highly dynamic environments.

## Acknowledgements

The authors are grateful to the anonymous reviewers for their valuable suggestions and comments to improve the quality of the paper.

## REFERENCES

[1] P. Fernández-Arias, D. Vergara, and J. A. Orosa, "A global review of PWR nuclear power plants," *Applied Sciences*, vol. 10, no. 13, p. 4434, 2020.

[2] Y. Liu, H. He, T. Zhang, and X. Liu, "Pressurized water reactor fuel corrosion-related unidentified deposit and its related safety issues–I. Corrosion product deposition and heat transfer," *Annals of Nuclear Energy*, vol. 208, p. 110758, 2024.

[3] J. Hui, S. Ge, J. Ling, and J. Yuan, "Extended state observer-based adaptive dynamic sliding mode control for power level of nuclear power plant," *Annals of Nuclear Energy*, vol. 143, p. 107417, 2020.

[4] Q. Ahmed and A. I. Bhatti, "Estimating SI engine efficiencies and parameters in second-order sliding modes," *IEEE Transactions on Industrial Electronics*, vol. 58, no. 10, pp. 4837-4846, 2010.

[5] J. Hui and J. Yuan, "Kalman filter, particle filter, and extended state observer for linear state estimation under perturbation (or noise) of MHTGR," *Progress in Nuclear Energy*, vol. 148, p. 104231, 2022.

[6] Z. Dong, M. Liu, Z. Guo, X. Huang, Y. Zhang, and Z. Zhang, "Adaptive state-observer for monitoring flexible nuclear reactors," *Energy*, vol. 171, pp. 893-909, 2019.

[7] G. Ansarifar, "Estimation of the poisons reactivity in the PWR Nuclear Reactors using modified higher order sliding mode observer based on the multi-point nuclear reactor model," *Annals of Nuclear Energy*, vol. 112, pp. 158-169, 2018.

[8] J. Zou, S. Liu, C. Jin, Y. Cai, L. Wang, and Y. Chen, "Optimization method of burnable poison based on genetic algorithm and artificial neural network," *Annals of Nuclear Energy*, vol. 192, p. 109985, 2023.

[9] Z. Dong, B. Li, J. Li, X. Huang, and Z. Zhang, "Online reliability assessment of energy systems based on a high-order extended-state-observer with application to nuclear

reactors," *Renewable and sustainable energy reviews*, vol. 158, p. 112159, 2022.
[10] A. Koul, "Development of data-driven method for capacity estimation and prognosis for lithium-ion batteries," 2020.
[11] M. Z. Ygane and G. Ansarifar, "Extended Kalman filter design to estimate the poisons concentrations in the PWR nuclear reactors based on the reactor power measurement," Annals of Nuclear Energy, vol. 101, pp. 576-585, 2017.
[12] S. Javadi and A. Hesami Naghshbandy, "Comparison of Dynamic State Estimation Methods in the Time Domain," *International Journal of Industrial Electronics Control and Optimization*, 2024.
[13] R. Havangi and M. Moradi, "PSO based EKF wheel-rail adhesion estimation," *International Journal of Industrial Electronics Control and Optimization*, vol. 6, no. 1, pp. 49-62, 2023.
[14] D. Henry and S. Ygorra, "Hydrazine Concentration Estimation in the Secondary Circuit of a Nuclear Power Plant: a IQC LPV approach," *IFAC-PapersOnLine*, vol. 58, no. 13, pp. 697-702, 2024.
[15] Y. Fang, M. Fei, and H. Qian, "Pressurized Water reactor power level control: A nonlinear generalized predictive control with extended Kalman filter method," *Nuclear Engineering and Technology*, p. 103147, 2024.
[16] J. Elfring, E. Torta, and R. Van De Molengraft, "Particle filters: A hands-on tutorial," *Sensors*, vol. 21, no. 2, p. 438, 2021.
[17] D. Hetrick, "Dynamics of Nuclear Reactors, American Nuclear Society," La Grange Park, IL, 1993.
[18] H. Eliasi, M. Menhaj, and H. Davilu, "Robust nonlinear model predictive control for a PWR nuclear power plant," Progress in Nuclear Energy, vol. 54, no. 1, pp. 177-185, 2012.
[19] H. Eliasi, "Design an anti-windup controller for a PWR power-level control in the presence of control rod speed saturation," Annals of Nuclear Energy, vol. 132, pp. 415-426, 2019.
[20] H. Parhizkari, M. Aghaie, A. Zolfaghari, and A. Minuchehr, "An approach to stability analysis of spatial xenon oscillations in WWER-1000 reactors," Annals of Nuclear Energy, vol. 79, pp. 125-132, 2015.
[21] C. An, F. C. Moreira, and J. Su, "Thermal analysis of the melting process in a nuclear fuel rod," Applied Thermal Engineering, vol. 68, no. 1-2, pp. 133-143, 2014.
[22] E. E. Lewis, Fundamentals of nuclear reactor physics. Elsevier, 2008.
[23] H. Liu, F. Hussain, C. L. Tan, and M. Dash, "Discretization: An enabling technique," Data mining and knowledge discovery, vol. 6, pp. 393-423, 2002.
[24] M. S. Grewal and A. P. Andrews, Kalman filtering: Theory and Practice with MATLAB. John Wiley & Sons, 2014.
[25] P. Kaniewski, "Extended Kalman filter with reduced computational demands for systems with non-linear measurement models," Sensors, vol. 20, no. 6, p. 1584, 2020.
[26] J. Elfring, E. Torta, and R. Van De Molengraft, "Particle filters: A hands-on tutorial," Sensors, vol. 21, no. 2, p. 438, 2021.
[27] E. Gasmi, M. A. Sid, and O. Hachana, "Nonlinear event-based state estimation using particle filter under packet loss," *ISA transactions*, vol. 144, pp. 176-187, 2024.

**Hossein Zahmatkesh** was born in Mashhad, Iran, in 1998. He received the B.Sc. degree in electrical engineering from Sadjad University, Mashhad, Iran, in 2021 and the M.Sc. degree in control engineering from the University of Birjand, Birjand, Iran, in 2024. His research interests include Control, Nonlinear Dynamic Systems, Power Systems, State Estimation, Filtering and Transient Stability in Load Following by Nuclear Power Plants.

**Hussein Eliasi** received the B.S. degree in electrical engineering from the Ferdowsi University of Mashhad (FUM), Iran, in 2001. He received the M.S. and the Ph.D. degrees in nuclear engineering from Amirkabir University of Technology (Tehran), Iran, in 2005 and 2011, respectively. He is currently an associate professor in the Faculty of Electrical Engineering at the University of Birjand, Iran. His research interests include Constrained Nonlinear Dynamics Systems, Robust Control, State Estimation and Filtering, Parameter Optimization of Model Predictive Control, Transient Stability in Power Systems and Load Following by Nuclear Power Plants.